

Nanorheology of active-passive polymer mixtures differentiates between linear and ring polymer topology

– Supplementary Information –

Andrea Papale*

SISSA - Scuola Internazionale Superiore di Studi Avanzati, Via Bonomea 265, 34136 Trieste, Italy

Jan Smrek†

Faculty of Physics, University of Vienna, Boltzmannngasse 5, A-1090 Vienna, Austria

Angelo Rosa‡

SISSA - Scuola Internazionale Superiore di Studi Avanzati, Via Bonomea 265, 34136 Trieste, Italy

(Dated: July 6, 2021)

MODEL AND METHODS: DETAILS

We give here additional details related to the polymer/nanoprobe model used in this work (Sec. S1) and the computational effort required for the simulations (Sec. S2). Then, we conclude (Sec. S3) by describing the mathematical details beyond the calculation of some observables considered in this work.

S1. COMPUTATIONAL MODEL FOR POLYMERS AND NANOPROBES

Polymer-polymer interactions consist of the following three terms:

- (i) The potential energy term accounting for monomer-monomer excluded volume interactions, which is expressed by the shifted and truncated Lennard-Jones (LJ) function:

$$U_{\text{LJ}}(r) = \begin{cases} 4\epsilon \left[\left(\frac{\sigma}{r}\right)^{12} - \left(\frac{\sigma}{r}\right)^6 + \frac{1}{4} \right] & r \leq r_c \\ 0 & r > r_c \end{cases} \quad (\text{S1})$$

Here, r is the spatial distance between monomers and the chosen cut-off distance $r_c/\sigma = 2^{1/6}$ ensures that only purely repulsive monomer-monomer interactions are effectively taken into account. The parameters ϵ and σ fix the energy and length scales units, respectively.

- (ii) The bond potential between monomers which are nearest-neighbours along the same polymer chain, which is expressed by the so called finitely extensi-

ble non-linear elastic potential (FENE):

$$U_{\text{FENE}}(r) = \begin{cases} -\frac{1}{2} \kappa_{\text{FENE}} R_0^2 \log \left(1 - (r/R_0)^2 \right) & r \leq R_0 \\ \infty & r > R_0 \end{cases} \quad (\text{S2})$$

Here, $\kappa_{\text{FENE}} \sigma^2/\epsilon = 30$ is the spring constant and $R_0/\sigma = 1.5$ is the maximum extension of the elastic FENE bond.

- (iii) The bending energy term controlling polymer stiffness, which is expressed by the following function:

$$U_{\text{bend}}(\theta) = \kappa_{\text{bend}} \left(1 - \frac{(\vec{r}_{i+1} - \vec{r}_i) \cdot (\vec{r}_i - \vec{r}_{i-1})}{|\vec{r}_{i+1} - \vec{r}_i| |\vec{r}_i - \vec{r}_{i-1}|} \right) \quad (\text{S3})$$

Here, \vec{r}_i is the coordinate of the i -th monomer along each given chain, numbered from one of the termini (for linear chains) or from an arbitrarily chosen monomer (for rings). In the latter case, periodic boundary conditions along the ring are tacitly assumed. The bending constant $\kappa_{\text{bend}}/\epsilon = 5$, corresponding to a Kuhn [1, 2] segment $\ell_K/\sigma = 10$ [3].

The polymer solutions are accompanied by the presence of nanoprobes of different diameters. In order to model the nanoprobe-nanoprobe and nanoprobe-polymer interactions, we have resorted to the phenomenological expressions introduced by Everaers and Ejtehadi [4] and employed in previous works [5–8]. In particular:

- (iv) Nanoprobe-nanoprobe (nn) interactions are described by the expression:

$$\begin{cases} U_{\text{nn}}(r) = U_{\text{nn}}^A(r) + U_{\text{nn}}^R(r) & r \leq r_{\text{nn}} \\ 0 & r > r_{\text{nn}} \end{cases} \quad (\text{S4})$$

$U_{\text{nn}}^A(r)$ is the attractive contribution given by

$$U_{\text{nn}}^A(r) = -\frac{A_{\text{nn}}}{6} \left[\frac{2a^2}{r^2 - 4a^2} + \frac{2a^2}{r^2} + \ln \left(\frac{r^2 - 4a^2}{r^2} \right) \right], \quad (\text{S5})$$

* andrea.papale@ens.psl.eu; Current affiliation: Group of Data Modeling and Computational Biology, IBENS-PSL École Normale Supérieure, Paris, France.

† jan.smrek@univie.ac.at

‡ anrosa@sissa.it

Quantity	Value
Correlation length, ξ/σ	1.4
Entanglement length, L_e/σ	11.0
Tube diameter, d_T/σ	4.3
Entanglement time, τ_e/τ_{MD}	490.0

TABLE S1. List of relevant length and time scales describing the microscopic properties of the polymer solution: (i) The correlation length, ξ , is defined as the average spatial distance from a monomer on one chain to the nearest monomer on another chain [2] and it is a measure of the packing of the solution; (ii) The entanglement length, L_e , can be defined as the contour length along a single chain which spans between close-by entanglement points in the solution [10, 11]; (iii) The tube diameter, $d_T \approx \sqrt{\ell_K L_e}$, measures the average span in length between close entanglement points along the same chain [10, 11]; (iv) The entanglement time, τ_e , is the average time for a monomer to explore by random motion a portion of the solution of linear size $= d_T$ [10, 11].

while $U_{\text{nn}}^B(r)$ is the repulsive term

$$U_{\text{nn}}^B(r) = \frac{A_{\text{nn}}}{37800} \frac{\sigma^6}{r} \left[\frac{r^2 - 14ar + 54a^2}{(r - 2a)^7} + \frac{r^2 + 14ar + 54a^2}{(r + 2a)^7} - 2 \frac{r^2 - 30a^2}{r^7} \right]. \quad (\text{S6})$$

Here, $A_{\text{nn}}/\epsilon = 39.478$ and we consider non-sticky, athermal probe particles with diameters $d/\sigma \equiv 2a/\sigma = 2.5, 5.0, 7.5$ corresponding to fix $r_{\text{nn}}/\sigma = 3.08, 5.60, 8.08$. As explained in great detail in Ref. [7] these nanoprobe diameters have been chosen because (a) they are larger than the *correlation length* [2] $\xi/\sigma \approx 1.4$ of the polymer solution while, at the same time, (b) they are able to span the entire range from below to above the estimated value $d_T/\sigma \approx 4.3$ of the *tube diameter* (see Table S1 for an overview of the physical property of the polymer solutions employed here). In this way, (a) polymer effects on nanoprobe displacement dominate [9] over thermal effects caused by the solvent and (b) the role of entanglements on nanoprobe motion can be explored more systematically.

- (v) Finally, the monomer-nanoprobe (mn) interaction is accounted for by:

$$\begin{cases} U_{\text{mn}}(r) = \frac{2a^3\sigma^3 A_{\text{mn}}}{9(a^2 - r^2)^3} \left[1 - \frac{5a^6 + 45a^4 r^2 + 63a^2 r^4 + 15r^6}{15(a-r)^6(a+r)^6} \right] & r \leq r_{\text{mn}} \\ 0 & r > r_{\text{mn}} \end{cases} \quad (\text{S7})$$

where $A_{\text{mn}}/\epsilon = 75.358$ and $r_{\text{mn}}/\sigma = 2.11, 3.36, 4.61$.

S2. MOLECULAR DYNAMICS RUNS

As explained in the main text, we have performed Langevin molecular dynamics for a polymer system made of $M = 80$ chains of $N = 500$ beads each and $N_{\text{np}} = 100$ nanoprobe dispersed in the solution. Simulations were performed by using the LAMMPS package [12]. Half of the chains are coupled to a thermostat with “room” temperature $T_c = T \equiv \epsilon/k_B$ (k_B being the Boltzmann constant) and the other half are coupled to a “hotter” thermostat with temperature $T_h/T_c > 1$. The nanoprobe are always coupled to the cold thermostat. By defining the “reduced” temperature gap $\Delta t \equiv T_h/T_c - 1$, we have considered systems with $T_h/T_c = 1.5$ or $\Delta t = 0.5$ and $T_h/T_c = 2.0$ or $\Delta t = 1.0$. Then, we have compared the properties of these systems to those for “purely passive” solutions with $T_h/T_c = 1.0$ or $\Delta t = 0.0$.

Polymers/nanoprobe mixtures are prepared and then let equilibrate under purely passive conditions according to the protocol described in detail in Ref. [7]. Starting from these equilibrated systems, half of the chains are then driven out of equilibrium by the coupling to the hot thermostat. The total length of each MD run is $\approx 4 \cdot 10^9$ integration time steps τ_{int} (with our choice $\tau_{\text{int}}/\tau_{\text{MD}} = 0.006$, this is equivalent to about $\approx 2.4 \cdot 10^7$ MD Lennard-Jones time units). System configurations are sampled each $10^5 \tau_{\text{int}} = 600 \tau_{\text{MD}}$: in order to remove possible artifacts due to the initial preparation of the samples, all the analyses reported in this work have been performed after discarding the first $5 \cdot 10^7 \tau_{\text{int}} = 3 \cdot 10^5 \tau_{\text{MD}}$ of each trajectory. For completeness and in order to investigate smaller time scales, we have also performed additional runs of total length $\approx 2 \cdot 10^6 \tau_{\text{int}} = 1.2 \cdot 10^4 \tau_{\text{MD}}$ with reduced sampling time of $100 \tau_{\text{int}} = 0.6 \tau_{\text{MD}}$.

As shown in Fig. S1, the runs are long enough for the mean-square displacement to be above the squared gyration radius. This is typically long enough to achieve the complete relaxation of polymer systems, see Ref. [13]. Table S2 summarizes the average temperature of the nanoprobe, $\langle T_{\text{np}} \rangle$, and the average temperatures of the monomers of cold and hot chains, $\langle T_{\text{ch}} \rangle^{c,h}$, after the complete relaxation of the corresponding systems. It reports also the corresponding values for the “temperature asymmetry” order parameters (see Ref. [14]) for hot chains with respect to nanoprobe ($\chi_{\text{np}}^h \equiv \frac{\langle T_{\text{ch}} \rangle^h}{\langle T_{\text{np}} \rangle} - 1$) and for hot chains w.r.t. cold chains ($\chi_c^h \equiv \frac{\langle T_{\text{ch}} \rangle^h}{\langle T_{\text{ch}} \rangle^c} - 1$).

In addition, we have performed a different run (of total length $= 1.2 \cdot 10^7 \tau_{\text{MD}}$) for a fully passive systems of ring polymers and large nanoprobe with diameter $d/\sigma = 7.5$. The system and numerical details are as before: the only exception is that now the bending stiffness of 50% of the chain population is as before ($\kappa_{\text{bend}}/\epsilon = 5.0$, see Sec. S1 here) while the remaining 50% of rings are twice more flexible with $\kappa_{\text{bend}}/\epsilon = 2.5$. By this protocol, the average chain sizes of the two populations of rings “fit” the sizes found for passive/active mixtures at $\Delta t = 1.0$ (see inset in Fig. 3 in the main paper).

		Linear Polymers					Ring Polymers				
d/σ	Δt	$\langle T_{\text{np}} \rangle$	$\langle T_{\text{ch}} \rangle^c$	$\langle T_{\text{ch}} \rangle^h$	χ_{np}^h	χ_c^h	$\langle T_{\text{np}} \rangle$	$\langle T_{\text{ch}} \rangle^c$	$\langle T_{\text{ch}} \rangle^h$	χ_{np}^h	χ_c^h
2.5	0.0	1.005 ± 0.073	1.000 ± 0.005	1.000 ± 0.005	$\approx 5 \cdot 10^{-2}$	$\lesssim 10^{-3}$	1.030 ± 0.082	1.000 ± 0.005	1.000 ± 0.005	$\approx 3 \cdot 10^{-2}$	$\lesssim 10^{-3}$
	0.5	1.200 ± 0.100	1.067 ± 0.006	1.432 ± 0.007	0.19 ± 0.02	0.342 ± 0.004	1.199 ± 0.094	1.059 ± 0.006	1.438 ± 0.008	0.20 ± 0.02	0.358 ± 0.004
	1.0	1.376 ± 0.119	1.127 ± 0.007	1.870 ± 0.011	0.36 ± 0.03	0.658 ± 0.008	1.359 ± 0.112	1.122 ± 0.007	1.877 ± 0.010	0.38 ± 0.03	0.672 ± 0.008
5.0	0.0	1.009 ± 0.087	1.000 ± 0.006	1.000 ± 0.006	$\approx 1 \cdot 10^{-2}$	$\lesssim 10^{-3}$	1.020 ± 0.083	1.000 ± 0.006	1.000 ± 0.006	$\approx 2 \cdot 10^{-2}$	$\lesssim 10^{-3}$
	0.5	1.191 ± 0.105	1.069 ± 0.006	1.431 ± 0.008	0.20 ± 0.02	0.339 ± 0.004	1.183 ± 0.104	1.060 ± 0.006	1.441 ± 0.009	0.22 ± 0.02	0.360 ± 0.004
	1.0	1.348 ± 0.100	1.138 ± 0.007	1.860 ± 0.012	0.38 ± 0.03	0.635 ± 0.008	1.323 ± 0.087	1.124 ± 0.007	1.877 ± 0.011	0.42 ± 0.03	0.669 ± 0.008
7.5	0.0	1.004 ± 0.076	0.999 ± 0.005	0.999 ± 0.005	$\approx 4 \cdot 10^{-3}$	$\lesssim 10^{-3}$	1.000 ± 0.077	1.000 ± 0.005	1.000 ± 0.005	$\lesssim 10^{-3}$	$\lesssim 10^{-3}$
	0.5	1.172 ± 0.093	1.075 ± 0.006	1.424 ± 0.008	0.21 ± 0.02	0.324 ± 0.004	1.120 ± 0.090	1.064 ± 0.007	1.436 ± 0.008	0.28 ± 0.02	0.349 ± 0.004
	1.0	1.292 ± 0.107	1.144 ± 0.007	1.856 ± 0.011	0.44 ± 0.04	0.623 ± 0.007	1.163 ± 0.095	1.125 ± 0.007	1.875 ± 0.011	0.61 ± 0.05	0.667 ± 0.008

TABLE S2. Summary of average temperatures for nanoprobe ($\langle T_{\text{np}} \rangle$) and for individual monomers of cold and hot chains ($\langle T_{\text{ch}} \rangle^{c,h}$), and corresponding “temperature asymmetry” order parameters for hot chains with respect to nanoprobe ($\chi_{\text{np}}^h \equiv \frac{\langle T_{\text{ch}} \rangle^h}{\langle T_{\text{np}} \rangle} - 1$) and for hot chains w.r.t. cold chains ($\chi_c^h \equiv \frac{\langle T_{\text{ch}} \rangle^h}{\langle T_{\text{ch}} \rangle^c} - 1$). Temperatures are measured in the course of the simulations by the LAMMPS [12] numerical engine used for this work (see Sec. S2). d is the nanoprobe diameter and Δt is the reduced temperature gap introduced in the system (see the main text and Sec. S2 for details).

S3. OBSERVABLES AND MEASURED PROPERTIES: DEFINITIONS

1. Single-chain structure

Let us define $\mathcal{O}_m(t)$, the value of the generic observable \mathcal{O} referring to the m -th chain in the solution and evaluated at time step t of a given MD run of total run-time = T_{MD} . Its mean value, $\langle \mathcal{O} \rangle^{c,h}$, is defined by the formula:

$$\langle \mathcal{O} \rangle^{c,h} \equiv \frac{1}{M/2} \sum_{m=1}^{M/2} \frac{1}{t_*} \int_{T_{\text{MD}}-t_*}^{T_{\text{MD}}} \mathcal{O}_m(t) dt, \quad (\text{S8})$$

where: (a) t_* corresponds to the time scale above which chains, having diffused more than their own size, have reached the steady state (see Fig. S1); (b) the subscripts on the brackets $\langle \cdot \rangle^{c,h}$ mean that separate averages have been taken for the two chain populations coupled to the two thermostats. In analogous manner, distinct averages have been considered in the case of chains with different flexibilities (Sec. S2).

In this work, we have considered the following single-chain observables for which we have computed corresponding mean values according to the definition (S8):

(i) The square gyration radius of a polymer chain made of N monomers, defined by:

$$R_g^2(t) \equiv \frac{1}{N} \sum_{i=1}^N (\vec{r}_i(t) - \vec{r}_{\text{cm}}(t))^2, \quad (\text{S9})$$

where: (a) $\vec{r}_i(t)$ is the spatial position of the i -th monomer of the chain at time t ; (b) $\vec{r}_{\text{cm}}(t) \equiv \frac{1}{N} \sum_{i=1}^N \vec{r}_i(t)$ is the position of the center of mass of the

		Linear Polymers		Ring Polymers	
d/σ	Δt	$\langle R_g^2 \rangle^h$	$\langle R_g^2 \rangle^c$	$\langle R_g^2 \rangle^h$	$\langle R_g^2 \rangle^c$
2.5	0.0	700.5 ± 62.7		167.7 ± 9.2	
	0.5	488.2 ± 32.5	615.2 ± 44.9	139.2 ± 7.5	170.4 ± 10.5
	1.0	391.7 ± 31.4	574.8 ± 47.8	128.7 ± 6.3	181.5 ± 10.0
5.0	0.0	690.9 ± 52.1		169.1 ± 9.4	
	0.5	486.8 ± 36.1	583.5 ± 41.4	138.1 ± 7.6	177.4 ± 10.0
	1.0	386.9 ± 28.5	576.6 ± 43.0	132.2 ± 7.6	189.0 ± 11.5
7.5	0.0	653.0 ± 39.7		174.7 ± 10.4	
	0.5	451.6 ± 33.2	577.7 ± 44.0	137.3 ± 7.5	193.6 ± 12.6
	1.0	368.6 ± 30.3	581.8 ± 43.8	129.6 ± 6.6	248.5 ± 9.4

TABLE S3. Mean-square gyration radii corresponding to the different chain population considered in this work. The superscript “c” (respectively, “h”) is for “cold” (resp. “hot”) chains in the melt. d is the nanoprobe diameter and Δt is the reduced temperature gap introduced in the system (see the main text and Sec. S2 for details). $\Delta t = 0$ is for classical passive melts and one single value is reported.

chain. The mean-square gyration radii for the different chain populations are reproduced in Table S3.

(ii) The average square end-to-end distance between two monomers at given contour length separation $\ell \in [\sigma, (N-1)\sigma]$ along the chain, defined by:

$$R^2(\ell \equiv n\sigma; t) \equiv \frac{1}{N-n} \sum_{i=1}^{N-n} (\vec{r}_{i+n}(t) - \vec{r}_i(t))^2, \quad (\text{S10})$$

where σ is the average bond length (see Sec. S1). Definition (S10) works for linear chains, the generalization

to rings (where $\ell \in [\sigma, N\sigma/2]$) is obtained by taking into account the obvious periodicity along the contour length of the chain.

2. Nanoprobe dynamics

To quantify the dynamics of single nanoprobes immersed in polymer solutions, we introduce the mean-square displacement, $\Delta r_{\text{np},i}^2(\mathcal{T}; \tau)$, for the i -th nanoprobe ($i = 1, \dots, N_{\text{np}} = 100$) as a function of the lag-time τ and the measurement time \mathcal{T} [7, 8, 15]:

$$\Delta r_{\text{np},i}^2(\mathcal{T}; \tau) \equiv \frac{1}{\mathcal{T} - \tau} \int_0^{\mathcal{T} - \tau} (\vec{r}_i(t + \tau) - \vec{r}_i(t))^2 dt, \quad (\text{S11})$$

with $\vec{r}_i(t)$ being the spatial position of the i -th nanoprobe at time t . By tacitly assuming that the simulated trajectories are long enough such that the “ $\mathcal{T} \rightarrow \infty$ ” limit is effectively reached, the time average mean-square displacement is formally given by:

$$\Delta r_{\text{np},i}^2(\tau) \equiv \lim_{\mathcal{T} \rightarrow \infty} \Delta r_{\text{np},i}^2(\mathcal{T}; \tau). \quad (\text{S12})$$

The average over the ensemble of N_{np} nanoprobes is then given by:

$$\langle \Delta r_{\text{np}}^2(\tau) \rangle \equiv \frac{1}{N_{\text{np}}} \sum_{i=1}^{N_{\text{np}}} \Delta r_{\text{np},i}^2(\tau). \quad (\text{S13})$$

In ergodic systems, Eq. (S12) should of course be independent from i . This, however, might not be the case whenever dynamics is affected by long-range spatial correlations as in glassy entangled polymer systems [15, 16] or polymer nanocomposites [7, 8]. To detect such effects, we have measured the following ratios:

$$\Delta r_{\text{np},i}^2(\mathcal{T}; \tau) / \langle \Delta r_{\text{np}}^2(\tau) \rangle \quad (i = 1, \dots, N_{\text{np}}). \quad (\text{S14})$$

Plots of the quantity Eq. (S14) are shown in Fig. S7.

Finally, motivated by the biased displacement orientation and following previous work [7, 8], we measure also the so called van-Hove [17] distribution function, $P(\tau; \Delta x)$, of the Cartesian components ($\alpha = x, y, z$) of nanoprobe spatial displacements for given lag-time τ :

$$P(\tau; \Delta x) \equiv \langle \delta[(r_\alpha(t + \tau) - r_\alpha(t)) - \Delta x] \rangle, \quad (\text{S15})$$

where δ is the Dirac's δ -function. For ordinary diffusion processes $P(\tau; \Delta x) = \frac{1}{\sqrt{2\pi \langle \Delta x^2 \rangle}} \exp\left(-\frac{\Delta x^2}{2 \langle \Delta x^2 \rangle}\right)$ is Gaussian, while correlated motion (*i.e.*, the one arising most typically in glassy and complex fluids [15, 17]) displays distributions with heavy tails. Results for $P(\tau; \Delta x)$ are shown in Fig. S8.

3. Single-chain dynamics

Similarly to Eqs. (S11) and (S12), we have considered the mean-square displacement, $g_{3,m}(\tau)$ [1, 18], of the centre of mass of the m -th chain in the solution:

$$g_{3,m}(\tau) = \lim_{\mathcal{T} \rightarrow \infty} \frac{1}{\mathcal{T} - \tau} \int_0^{\mathcal{T} - \tau} (\vec{r}_{\text{cm},m}(t + \tau) - \vec{r}_{\text{cm},m}(t))^2 dt, \quad (\text{S16})$$

where $\vec{r}_{\text{cm},m}(t)$ is the coordinate of the centre of mass of the m -th chain. As in static quantities (Sec. S3 1), we take distinct averages of Eq. (S16) for the two polymer populations with the cold/hot thermostat (see Fig. S1):

$$g_3^{\text{c,h}}(\tau) = \frac{1}{M/2} \sum_{m=1}^{M/2} g_{3,m}(\tau). \quad (\text{S17})$$

-
- [1] M. Doi and S. F. Edwards, *The Theory of Polymer Dynamics* (Oxford University Press, New York, 1986).
- [2] M. Rubinstein and R. H. Colby, *Polymer Physics* (Oxford University Press, New York, 2003).
- [3] A. Rosa and R. Everaers, *Plos Comput. Biol.* **4**, e1000153 (2008).
- [4] R. Everaers and M. R. Ejtehadi, *Phys. Rev. E* **67**, 041710 (2003).
- [5] M. Valet and A. Rosa, *J. Chem. Phys.* **141**, 245101 (2014).
- [6] N. Nahali and A. Rosa, *J. Phys.-Condens. Matter* **28**, 065101 (2016).
- [7] N. Nahali and A. Rosa, *J. Chem. Phys.* **148**, 194902 (2018).
- [8] A. Papale and A. Rosa, *Phys. Biol.* **16**, 066002 (2019).
- [9] T. Ge, J. T. Kalathi, J. D. Halverson, G. S. Grest, and M. Rubinstein, *Macromolecules* **50**, 1749 (2017).
- [10] R. Everaers, S. K. Sukumaran, G. S. Grest, C. Svaneborg, A. Sivasubramanian, and K. Kremer, *Science* **303**, 823 (2004).
- [11] N. Uchida, G. S. Grest, and R. Everaers, *J. Chem. Phys.* **128**, 044902 (2008).
- [12] S. Plimpton, *J. Comp. Phys.* **117**, 1 (1995).
- [13] J. D. Halverson, W. B. Lee, G. S. Grest, A. Y. Grosberg, and K. Kremer, *J. Chem. Phys.* **134**, 204905 (2011).
- [14] J. Smrek and K. Kremer, *Phys. Rev. Lett.* **118**, 098002 (2017).
- [15] D. Michieletto, N. Nahali, and A. Rosa, *Phys. Rev. Lett.* **119**, 197801 (2017).
- [16] J. Smrek, I. Chubak, C. N. Likos, and K. Kremer, *Nat. Commun.* **11**, 26 (2020).
- [17] P. Chaudhuri, L. Berthier, and W. Kob, *Phys. Rev. Lett.* **99**, 060604 (2007).
- [18] K. Kremer and G. S. Grest, *J. Chem. Phys.* **92**, 5057 (1990).
- [19] C. Svaneborg and R. Everaers, *Macromolecules* **53**, 1917 (2020).
- [20] Y. Rabin and A. Y. Grosberg, *Macromolecules* **52**, 6927 (2019).

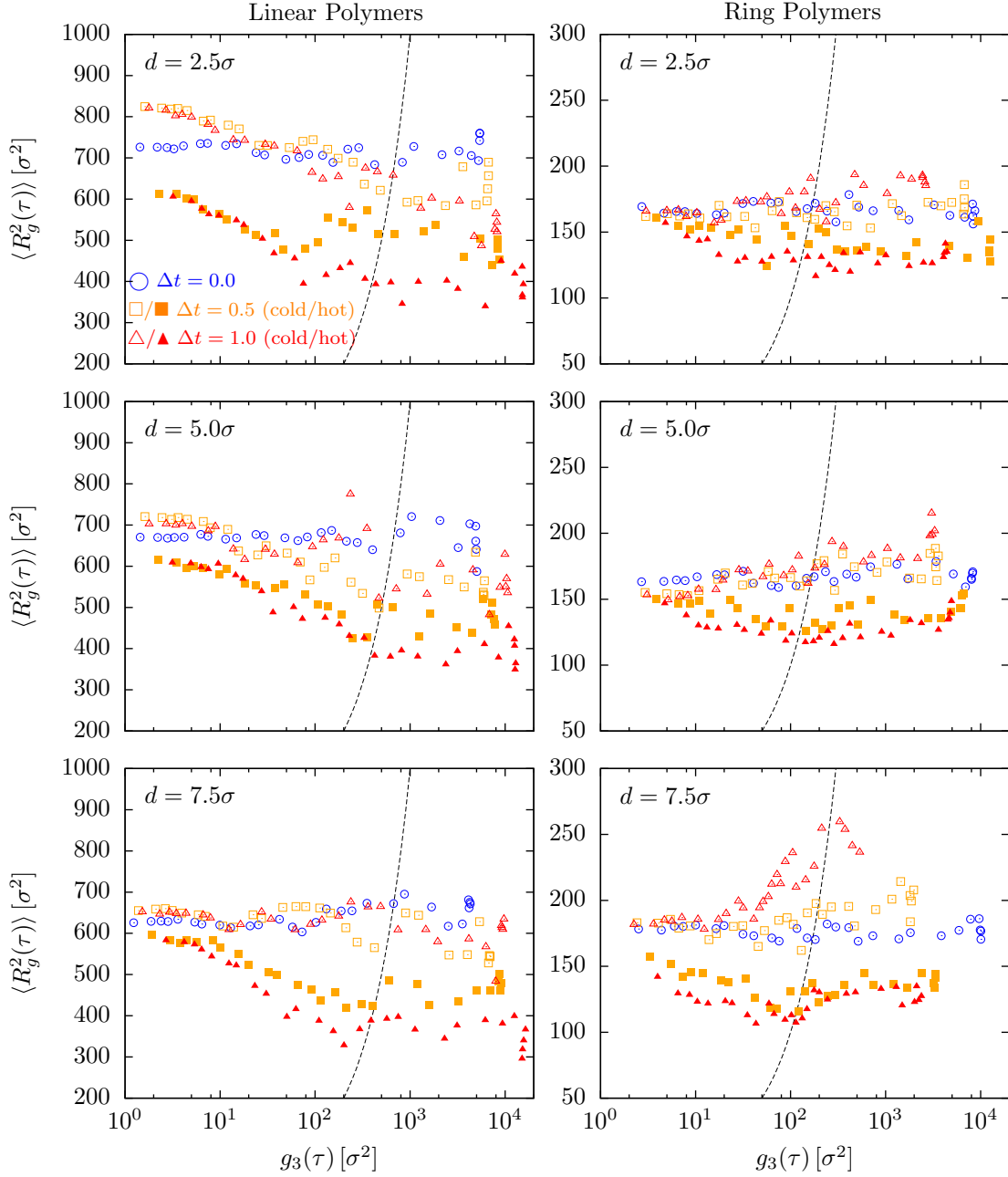


FIG. S1. Parametric plot of the time evolution of the chain mean-square gyration radius, $\langle R_g^2(\tau) \rangle$ (average of Eq. (S9) on the ensemble of chains coupled to the same temperature T for the single MD snapshot at time τ), as a function of the mean-square displacement, $g_3(\tau)$ (Eq. (S17)), of the chain center of mass. The black dashed lines mark the positions where $g_3 = \langle R_g^2 \rangle$, hence points to the right of the line demonstrate that the systems were run long enough to reach polymer displacements larger than the chain average gyration radius. Color code is as in the main paper, with different colors corresponding to reduced temperatures $\Delta t = 0.0, 0.5, 1.0$. Open/full symbols correspond to chains coupled to the cold/hot thermostat in passive/active mixtures (see legend).

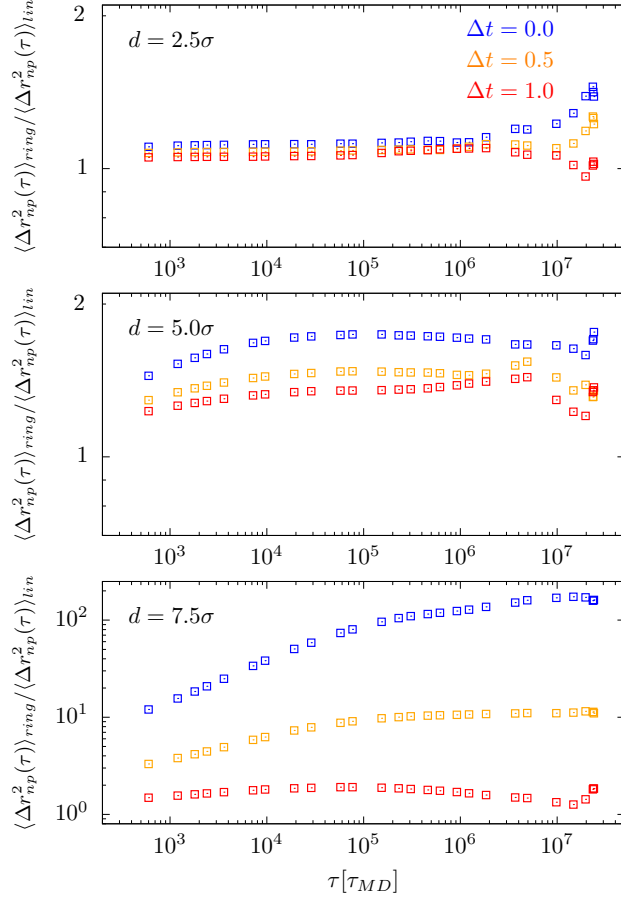


FIG. S2. $\langle \Delta r_{np}^2(\tau) \rangle_{ring} / \langle \Delta r_{np}^2(\tau) \rangle_{lin}$, ratios of nanoprobe mean-square displacements (Eq. (S13)) in rings *vs.* linear polymer solutions. Results for increasing nanoprobe diameters d (from top to bottom). Color code is as in the rest of the paper. Although diffusion in ring solutions is always larger than diffusion in linear solutions, for $d = 2.5\sigma$ and $d = 5.0\sigma$ we notice a small yet clearly visible slow-down of the nanoprobes at increasing Δt . Since the measured average temperatures of the nanoprobes are the same for the same Δt (*i.e.*, they do not depend on polymer architecture, see Table S2), we are tempted to ascribe this effect to the dependence of entanglements on chain flexibility [11, 19]. In fact, in active-passive mixtures hot and cold chains of linear solutions are both more flexible than chains in fully passive counterparts (Figs. S3 and S4, l.h.s. panels) while in ring solutions (Fig. S3 and S4, r.h.s. panels) only hot chains bend more: since more/less flexible chains are in general associated to less/more entangled polymers [11, 19] this may finally account [9, 20] for the seen acceleration/deceleration of the nanoprobes. On the other hand, this explanation sits on a definition of “entanglements” introduced and validated only for equilibrium system: if it remains valid for out-of-equilibrium polymer solutions remains to be established, and more systematic investigations ought to be pursued in the future in this respect.

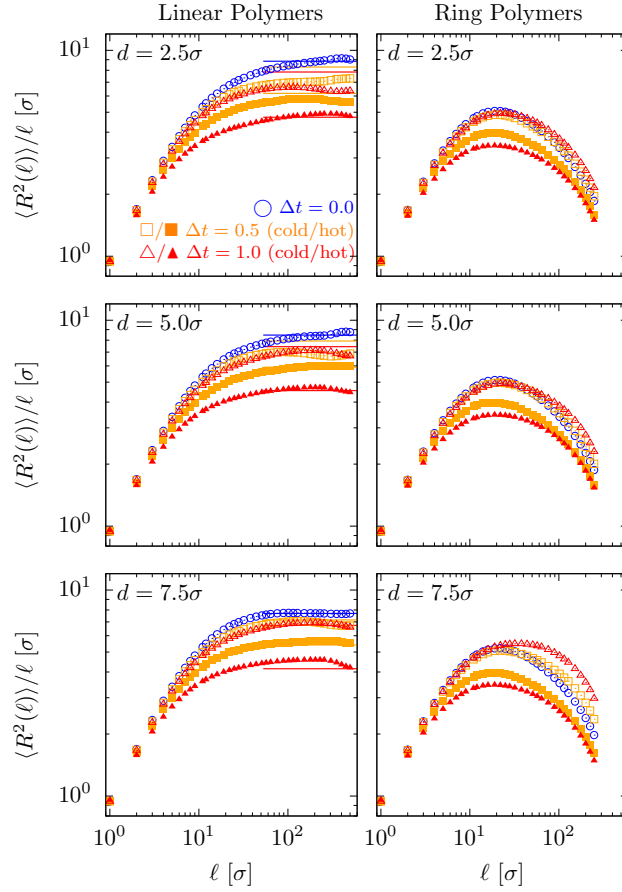


FIG. S3. $\langle R^2(\ell) \rangle / \ell$, mean-square end-to-end distances (Eq. (S10)) of linear chains (l.h.s. panels) and rings (r.h.s. panels) normalized to corresponding monomer-monomer contour distances ℓ . Color code is as in the rest of the paper and choice of the symbols is as in Fig. S1. For linear chains, the values of the plateaus at large ℓ , $\ell_K \equiv \lim_{\ell \rightarrow \infty} \langle R^2(\ell) \rangle / \ell$, correspond to the Kuhn lengths of the respective chains [1]: the horizontal lines show results based on the formula $\ell_K \langle \langle T_{\text{ch}} \rangle^{c,h} \rangle \equiv \frac{\ell_K(\Delta t=0)}{\kappa_B \langle T_{\text{ch}} \rangle^{c,h} / \epsilon}$, where $\ell_K(\Delta t = 0)$ comes from best fits of the passive-chain plateaus (on the interval $\ell/\sigma > 100$) and $\langle T_{\text{ch}} \rangle^{c,h}$ are the measured temperatures of cold/hot chains (see Table S2).

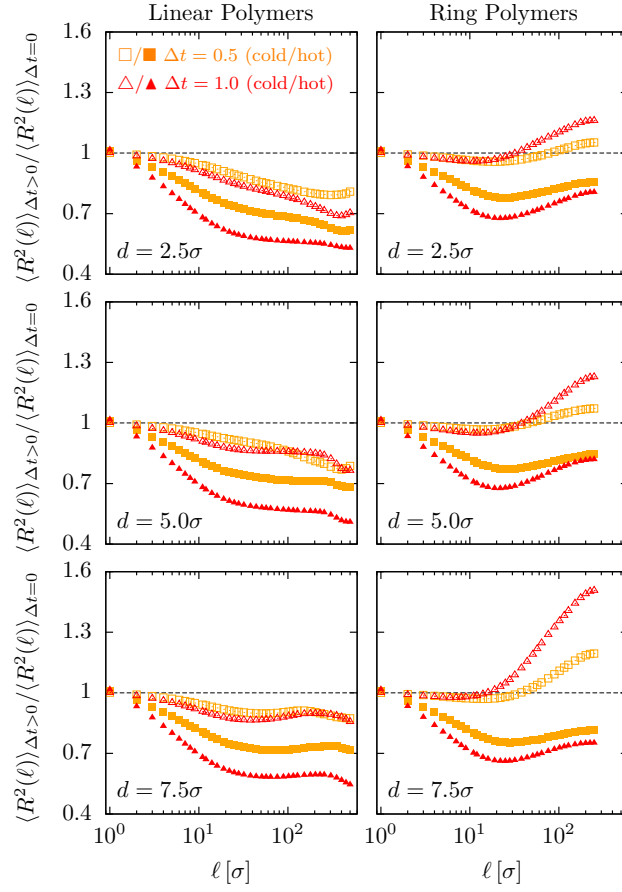


FIG. S4. $\langle R^2(\ell) \rangle_{\Delta t > 0} / \langle R^2(\ell) \rangle_{\Delta t = 0}$, mean-square end-to-end distances (Eq. (S10)) as a function of the monomer-monomer contour distance ℓ for linear chains (l.h.s. panels) and rings (r.h.s. panels) in passive/active mixtures normalized with respect to the corresponding quantity measured in passive systems. Color code is as in rest of the paper and choice of the symbols is as in Fig. S1.

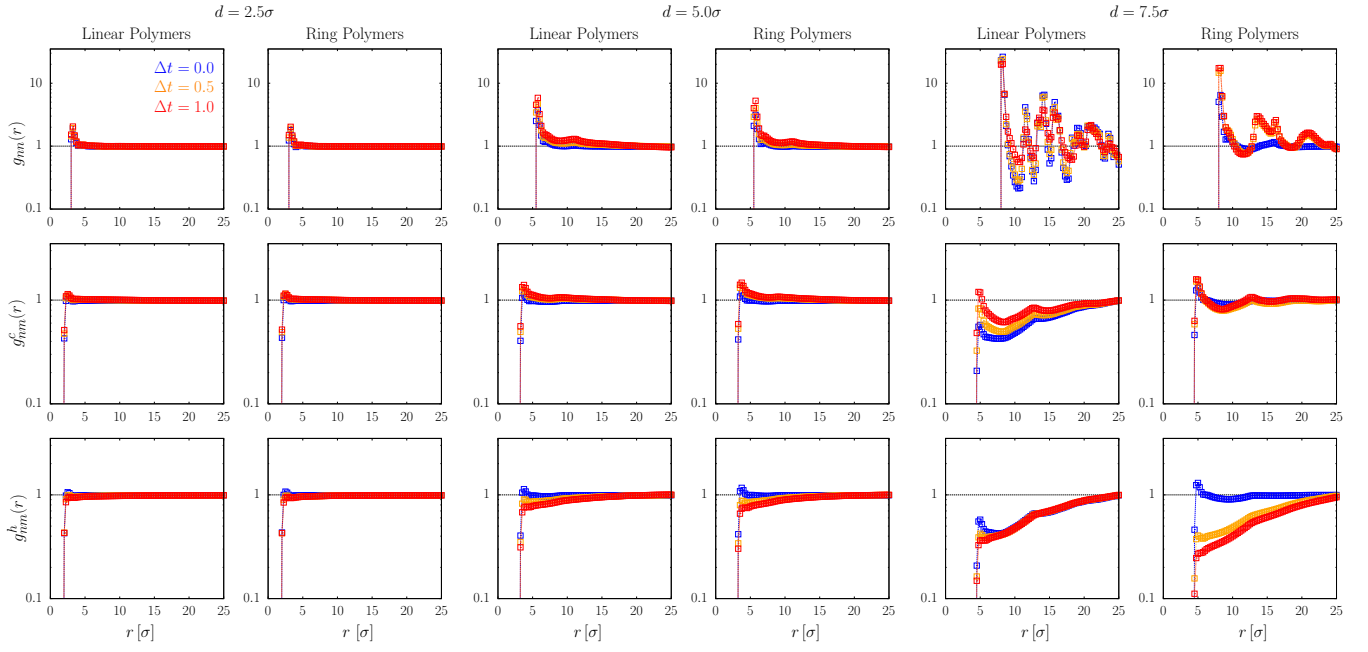


FIG. S5. Nanoprobe-nanoprobe ($g_{nn}(r)$) and nanoprobe-monomer ($g_{nm}^c(r)$ and $g_{nm}^h(r)$) pair correlation functions for nanoprobes of diameters $d/\sigma = 2.5, 5.0, 7.5$ (see legends). The superscripts indicate that the functions have been evaluated by separating the contributions of monomers coupled to the cold (c) or the hot (h) thermostat. Color code is as in rest of the paper.

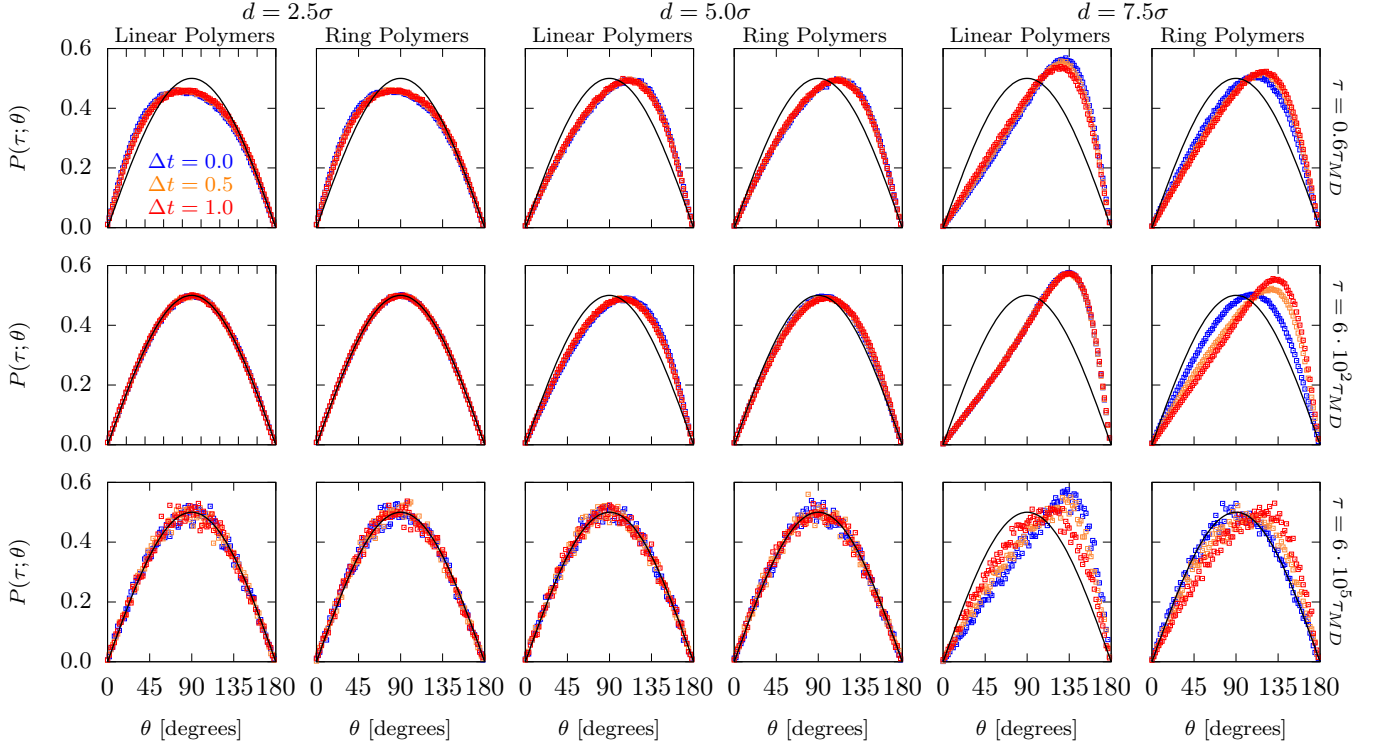


FIG. S6. Probability distribution functions, $P(\tau; \theta)$ (see Eq. (3) in the main paper), of the angle θ between oriented spatial displacements of nanoprobe diameters $d/\sigma = 2.5, 5.0, 7.5$ and selected lag-times $\tau/\tau_{MD} = 6 \cdot 10^{-1}, 10^2, 10^5$ (see legends). Color code is as in the rest of the paper. The black solid line is the function $P(\tau; \theta) = \frac{1}{2} \sin \theta$ for randomly oriented vectors.

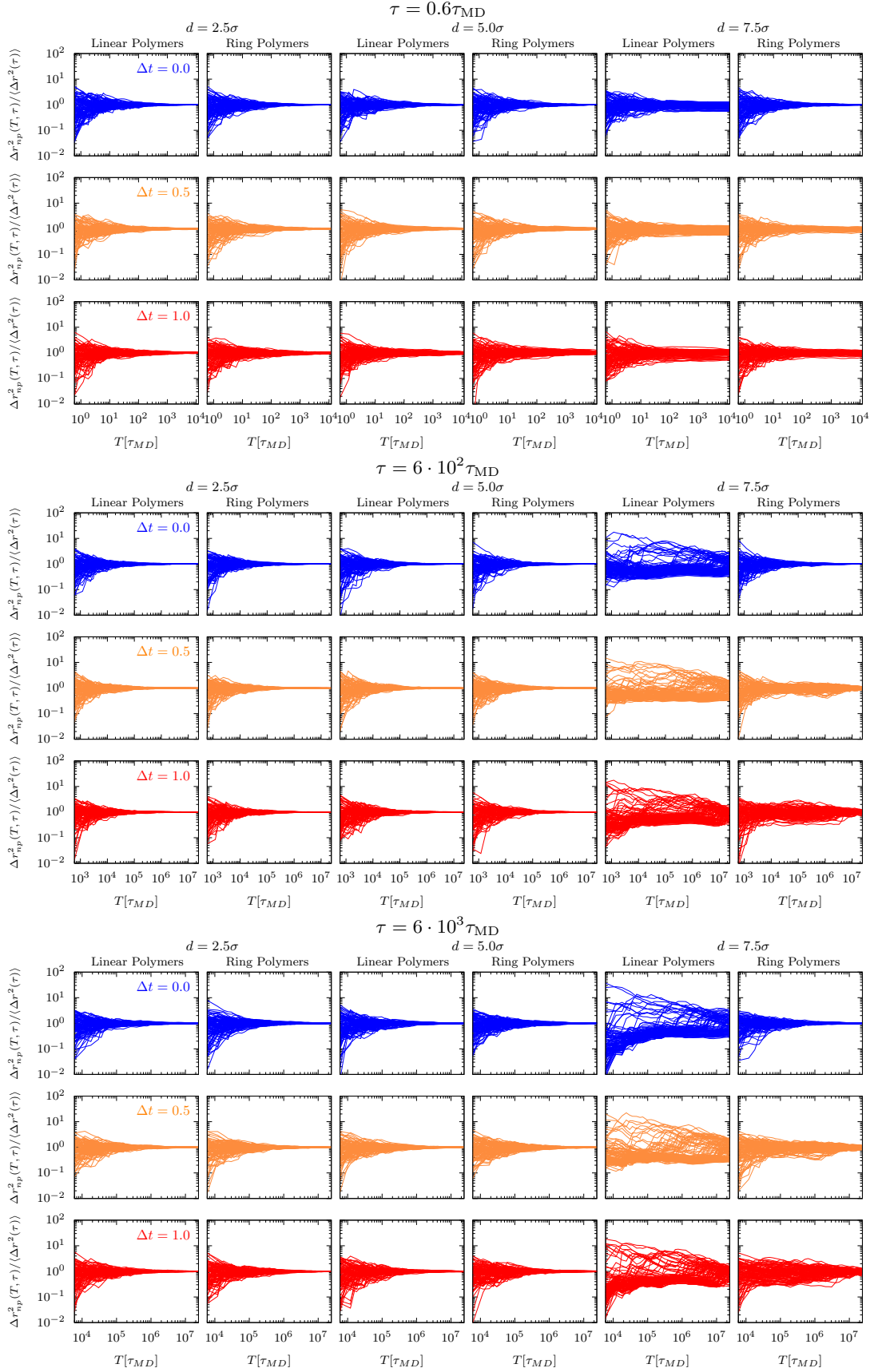


FIG. S7. Spatial heterogeneity, $\Delta r_{np,i}^2(T;\tau)/\langle\Delta r^2(\tau)\rangle$ (Eq. (S14)), of nanoprobe mean-square displacements *vs.* the measurement time \mathcal{T} for lag-times $\tau/\tau_{MD} = 6 \cdot 10^{-1}, 10^2, 10^3$ and nanoprobe diameters $d/\sigma = 2.5, 5.0, 7.5$ (see legends). Each panel here contains $N_{np} = 100$ curves. Color code is as in the rest of the paper.

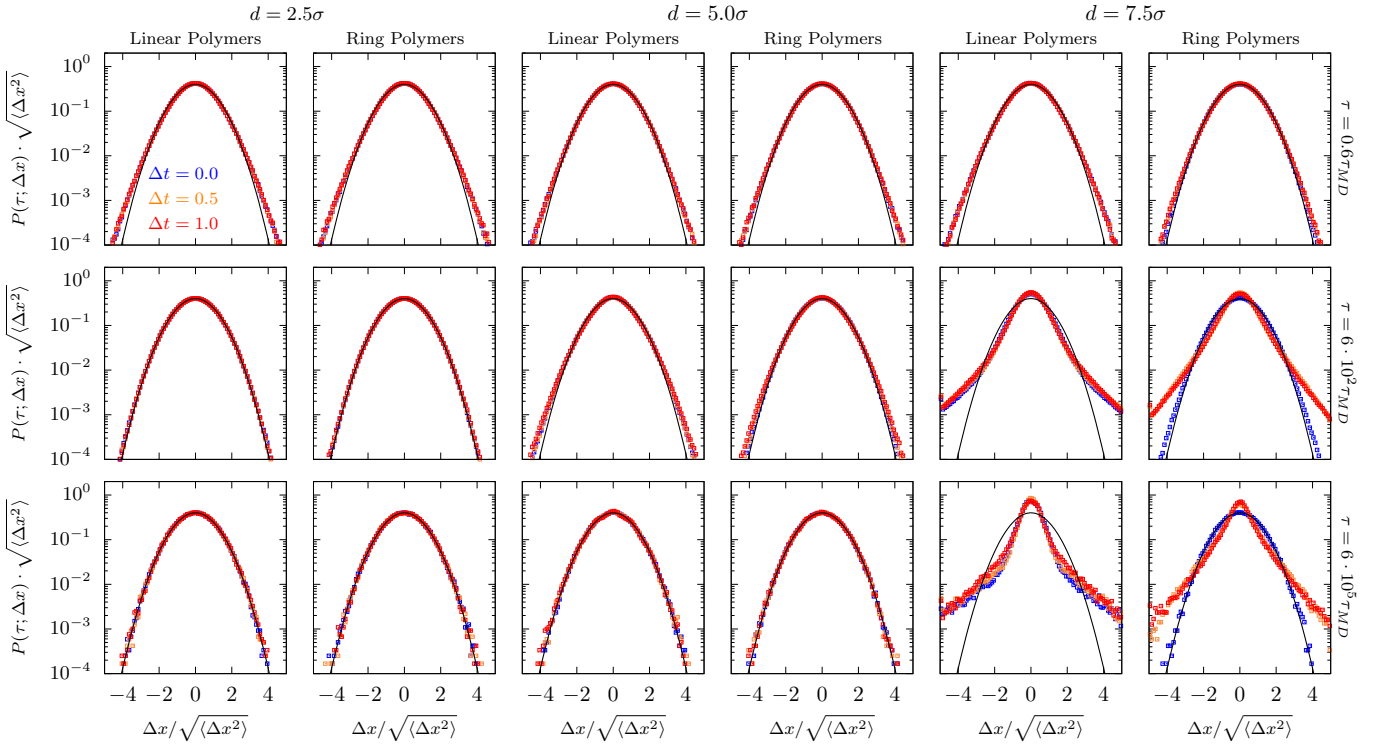


FIG. S8. Probability distribution functions of one-dimensional nanoprobe displacements, $P(\tau; \Delta x)$ (Eq. (S15)), for the same representative lag-times τ as in Fig. S6 and nanoprobe diameters $d/\sigma = 2.5, 5.0, 7.5$ (see legends). Color code is as in the rest of the paper. Black solid lines correspond to the theoretical Gaussian distribution function, $P(\Delta x) = \frac{1}{\sqrt{2\pi\langle\Delta x^2\rangle}} \exp\left(-\frac{\Delta x^2}{2\langle\Delta x^2\rangle}\right)$, which is typical for ordinary diffusive processes.